Hindawi
Security and Communication Networks
Volume 2023, Article ID 9820397, 1 page
https://doi.org/10.1155/2023/9820397

Retraction

Retracted: Research on Inversion of Suspended Sediment Concentration in Estuary Surface Based on Remote Sensing and GIS

Security and Communication Networks

Received 11 July 2023; Accepted 11 July 2023; Published 12 July 2023

This article has been retracted by Hindawi following an investigation undertaken by the publisher [1]. This investigation has uncovered evidence of one or more of the following indicators of systematic manipulation of the publication process:

(1) Discrepancies in scope
(2) Discrepancies in the description of the research reported
(3) Discrepancies between the availability of data and the research described
(4) Inappropriate citations
(5) Incoherent, meaningless and/or irrelevant content included in the article
(6) Peer-review manipulation

The presence of these indicators undermines our confidence in the integrity of the article's content and we cannot, therefore, vouch for its reliability. Please note that this notice is intended solely to alert readers that the content of this article is unreliable. We have not investigated whether authors were aware of or involved in the systematic manipulation of the publication process.

Wiley and Hindawi regrets that the usual quality checks did not identify these issues before publication and have since put additional measures in place to safeguard research integrity.

We wish to credit our own Research Integrity and Research Publishing teams and anonymous and named external researchers and research integrity experts for contributing to this investigation.

The corresponding author, as the representative of all authors, has been given the opportunity to register their agreement or disagreement to this retraction. We have kept a record of any response received.

References

[1] M. Zeng, J. Peng, and F. Liu, "Research on Inversion of Suspended Sediment Concentration in Estuary Surface Based on Remote Sensing and GIS," *Security and Communication Networks*, vol. 2022, Article ID 7795873, 8 pages, 2022.

Hindawi
Security and Communication Networks
Volume 2022, Article ID 7795873, 8 pages
https://doi.org/10.1155/2022/7795873

Research Article

Research on Inversion of Suspended Sediment Concentration in Estuary Surface Based on Remote Sensing and GIS

Ming Zeng,[1,2] Jun Peng ,[3] and Fucheng Liu[4]

[1]*College of Resource & Environment, Jiujiang University, Jiujiang 332005, China*
[2]*Jiangxi Key Laboratory of Industrial Ecological Simulation and Environmental Health in Yangtze River Basiny, Jiujiang 332005, China*
[3]*School of Geographic Information and Tourism, Chuzhou University, Chuzhou 239000, China*
[4]*School of Marine Technology and Geomatics, Jiangsu Ocean University, Lianyungang 222005, China*

Correspondence should be addressed to Jun Peng; pj_0519@chzu.edu.cn

Received 26 April 2022; Revised 28 May 2022; Accepted 9 June 2022; Published 31 July 2022

Academic Editor: Mukesh Soni

The concentration of suspended sediments at the estuarine surface (SSC) is a crucial indicator for monitoring water bodies. Given the current situation in which SSC remote sensing inversion is primarily based on low-resolution satellites, this study first discusses remote sensing and GIS technologies before employing the Sentinel-2 satellite, whose resolution can exceed 10 m after resampling. Inversion and comparison of SSC content during wet and dry periods. In addition, based on the neural network's ability to compensate for the inherent errors of traditional empirical techniques, this study designs and develops an artificial neural network-based neural network corrector to perform secondary correction on the empirical inversion results. In this study, the B2, B3, B4, and B8 inversion models are used to generate the sensitive bands, and the ratio of these bands is used to generate the inversion model. The results indicate that the model has a high level of precision, which can aid in reducing the model's inherent error and ensuring inversion precision.

1. Introduction

The sediment transport coefficient (STC) of a river is one of the most significant indicators of the river's water quality, and it is a fundamental hydrological phenomenon in a river. In water bodies, SSC influences a variety of optical qualities, including river color, water turbidity, and water transparency, among others and consequently impacts the biological habitat of aquatic species, such as photosynthesis, primary production, nutrient flow, and river biodiversity. It is common knowledge that constructing a dam in a natural river will raise the water level upstream. However, the flow rate will be reduced and suspended material in the river will accumulate at or near the dam's base. Due to sediment pressure, the dam's stress distribution may become unequal, resulting in structural and structural stability issues within the dam body [1–3]. As a result, while building dams in rivers with high SSC concentration, the impact of stress should be taken into consideration. The sediment content of the river also has a significant impact on the balance of the river channel, and local sediment deposition produces difficulties such as the deformation of the river bed. As a result, it is extremely important for the dynamic monitoring of SSC. SSC is traditionally measured by monitoring the sample sites one by one for a lengthy period of time in the sampling region, which is the conventional approach. However, this technology is not only time-consuming, but it also has other drawbacks, such as a high cost and the difficulty to monitor huge bodies of water for an extended period of time. Remote sensing technology offers a large monitoring range, requires little time and is very inexpensive when it comes to remote sensing picture collecting. The application of remote sensing technology to monitor river SSC has emerged as a new development trend in recent years. Because of limitations imposed by several factors such as the resolution of remote sensing pictures, the inversion of SSC by remote sensing

technology has been limited to surface water bodies such as seas and lakes, with just a few studies conducted on river linear water bodies.

Because of the optical reflectance, scattering, and absorption of various substances, different optical properties of the surface reflectance have the significant ability to extract information about the water quality parameters from the surface reflectance measurements. As computer calculating technology progresses, as well as the development of remote sensing technology, particularly spaceborne optical sensors, it is becoming possible to get water quality parameters (WOPs) with a greater spatial range and a better degree of precision [4–6].

The suspended sediment concentration (SSC) is an extremely important parameter for water monitoring because it is a consequence of aquatic degradation and soil erosion caused by deforestation and urbanization. In the majority of instances, the SSC is defined as the total concentration (in grams per liter or milligrams per liter) of both organic and inorganic particles suspended in the water due to turbulence. Total suspended solids (TSSs), in addition to total suspended matter (TSM) and suspended particulate matter (SPM) [4], are terms used to describe SSC (TSS). Due to the correlation between SSC and turbidity, it is simple to locate a specific landmark with known transparency on a map and evaluate the retrieval accuracy of the data. The historical evolution of retrieval methods for WQPs from remotely sensed data has produced three primary techniques: analytical, semi-analytical, and empirical approaches, in that order [7, 8]. In recent years, empirical algorithms have gained popularity due to the ease with which they may be implemented and the fact that they need less fieldwork. An empirical method that was widely used and developed early in the IOCCG. In order to adjust for the intensity variation of the light at various locations, the color-ratio method is based on the exponential function and band ratio of reflectance. For moderately turbid waters, some researchers have presented an empirical algorithm based on the band ratio between 670 and 555 nm for remote sensing reflectance, which has been found to be highly correlated. This algorithm was designed for moderately turbid waters and was developed by some researchers. In some cases, academics have suggested that the use of a single band method can also produce reliable results if the band is chosen correctly [9, 10].

To address the current situation in which the majority of remote sensing inversions of SSC use low-resolution satellites, this paper first introduces remote sensing and GIS technology before utilizing the Sentinel-2 satellite with a resolution of 10 m after resampling to conduct a comparative inversion study of SSC content in the upper reaches of a Chinese water conservancy hub during abundant and dry periods. In addition, a nerve network corrector based on an artificial nerve network is constructed and built to perform secondary correction on the inversion results, as a result of the nerve network's ability to compensate for the inherent flaws of the conventional algorithm.

2. Related Work

Climate, land use, and human activity have a significant impact on the composition and optical characteristics of second-class water bodies. As a result, an inversion model for general, high-precision suspended sediment cannot be developed at this time. Several researchers have proposed classifying water bodies with similar optical properties and developing a unique inversion model for each type of water body in order to improve its inversion accuracy. These proposals have produced promising results and helped overcome the time and space constraints of the watercolor parameter inversion algorithm for the two types of water bodies. On the basis of in situ observation data from Taihu Lake, some researchers have performed an optical classification of the lake's water, and on the basis of this classification, they have developed a total SSC hyperspectral inversion model that is applicable to various types of water. According to the findings, both the accuracy and stability of the inversion model increased following classification [8, 11–13]. Other researchers have developed classification-based total SSC inversion models for Taihu Lake using Environment-1, which also demonstrates that the classification-based method may significantly enhance the accuracy of inversion estimation. According to some researchers, the Ward algorithm was used to categorize spectral data of water bodies collected from 211 stations in the waters of the eastern English Channel, southern North Sea, and French Guiana collected over different seasons into four categories. The classification-based inversion was demonstrated by the estimation of the SSC. Whether the technique has the potential to improve the retrieval of ocean color products, and whether this class-specific algorithm can be applied to satellite information are both under investigation [14–17].

The SSC distribution, suspended sediment front, and temperature front in Chinese waters have all been studied extensively by a number of academics and researchers. A number of researchers have used the turbidity data from the North Yellow Sea in winter and summer to obtain the large-scale distribution of suspended matter through the linear fitting, and they have concluded that the different wind fields cause obvious seasonal differences in the distribution characteristics and transport mechanism of suspended matter in water [18]. Researchers have inverted SSC in the Yellow Sea using monthly average MODIS data, and they believe that the transport of suspended sediment exhibits significant seasonal variation characteristics and that the strong winds and waves as well as coastal currents in winter cause high SSC values in certain areas of the sea area. Researchers have investigated the characteristics of the offshore temperature front's distribution and changing laws [19–24]. They have also looked into the morphology, evolution and causes of the offshore temperature front. The SSC of the surface layer of the Yellow Sea and East China Sea was inverted using SeaWiFS satellite data, which was then utilized in conjunction with a Sobel algorithm to produce the suspended sediment front in the Yellow Sea and East China Sea. The most important governing factor is the drastically altered circulation structure between the winter and summer

months. Through tidal current observations and suspended matter flow estimates, some researchers have demonstrated that some suspended materials can be transported over the ocean current shear front produced by the coastal current and the Yellow Sea warm current. There is a water barrier, and the process by which it is transported is studied separately [25–27].

Some researchers have developed mathematical models to investigate the single-band reflectance and observed SSC of remote sensing satellites, nevertheless, the single-band inversion model is unable to rule out interference from chlorophyll and other compounds present in the environment. In remote sensing, some researchers have used the random forest regression model to estimate SSC, however, the machine model requires a large number of training samples, making it difficult to employ in the quantitative inversion of river remote sensing [28, 29]. Some researchers have used LandsatETM + remote sensing images to perform remote sensing inversions of suspended sediment in the middle reaches of the Yangtze River and to apply remote sensing technology to the monitoring of suspended sediment in linear water bodies; however, the image resolution of this method is 30 m lower than that of the previous method [30]. This article makes use of Sentinel-2 satellite data, which has a remote sensing picture resolution of 10 meters and a high level of detail.

Recently, with the advancement of processing power and the development of machine learning technologies, it has been possible to handle quite complicated WQP retrieval issues. The use of artificial intelligence technology has the benefit of obtaining a variety of water parameters using a single machine learning method, which is quite convenient. WQP inversion issues have been successfully solved by several machine learning methods including multi-linear regression, support vector machine, and artificial neural network (ANN) [1, 3, 7, 12, 14]. All of these techniques have proven accurate when applied to WQP inversion problems. Some studies used the least squares support vector machine parameterized by particle swarm optimization to estimate SSC from hyperspectral images captured by unmanned aerial vehicles (UAVs). Several researchers assert that retrieval potential can be evaluated by comparing multiple machine learning methods. In addition, they retrieved the relative variable importance, which indicates the need for additional research. Despite their black-box nature and difficulty in deconstruction, machine learning techniques are widely and successfully used in the remote sensing retrieval of WQPs [31–35].

3. Method

The Songhua River in China is used in this paper in relation to the specific research object. It is the largest urban wetland in China due to the abundance of wetland reserves in the vicinity of the Songhua River. It contains nearly 10,000 hectares of reed marshes, grasslands, and meadows, making it China's largest urban wetland. On certain stretches of the Songhua, it is possible to navigate the river for more than 200 days. During the dry season, the 1,000-ton fleet can also travel unimpeded on the Songhua River segment between the provinces of Harbin and Hebei. For quantitative inversion of river remote sensing, the river surface is widened, and the satellite sensor is adequate for identifying the river surface target, which is suitable for this field sampling region. [36].

The Songhua River in China is used in this paper in relation to the specific research object. It is the largest urban wetland in China due to the abundance of wetland reserves in the vicinity of the Songhua River. It contains nearly 10,000 hectares of reed marshes, grasslands, and meadows, making it China's largest urban wetland. On certain stretches of the Songhua, it is possible to navigate the river for more than 200 days. During the dry season, the 1,000-ton fleet can also travel unimpeded on the Songhua River segment between the provinces of Harbin and Hebei. For quantitative inversion of river remote sensing, the river surface is widened, and the satellite sensor is adequate for identifying the river surface target, which is suitable for this field sampling region. The sampling location for this article is shown in Figure 1.

Prior to taking field measurements, inspect the container and filter membrane associated with each sampling site to ensure that they are in good working order before proceeding. 500 mL wide-mouth plastic bottle serves as the container. In order to eliminate mistakes and to facilitate data screening, the depth of field sampling water is 0.5 m, and each sampling site gathers three bottled water samples. This is done in order to reduce the penetration of each wave band into the water body. A laboratory is used to examine and analyze the water samples once they have been collected. For the SSC of each sample station throughout the dry and wet seasons, as shown in Tables 1 and 2.

Sentinel-2 satellites were the source of all remote sensing data used in this article. On May 1, the actual measurement time is approximately 16:00, and on August 1, it is approximately 16:00. On 12 May and 1 August, Beijing time is 8:00 a.m., which is the same as New York time. Reduce the error resulting from the time difference between 8:00 and 9:00 a.m. The acquired cloud cover rates of 3.45 percent and 6.72 percent are both less than 10 percent, and the visibility is high, allowing the development of an inversion model.

Because the processed L2A data of the Sentinel-2 satellite does not contain remote sensing images corresponding to the actual sampling time of this time, the Sentinel-2 satellite data is downloaded from L1C-level products, which have undergone geometric correction but not radiometric calibration or atmospheric correction. Preparing remote sensing data for additional analysis. Sen2cor is utilized to process the L1C-level data to obtain the L2A-level atmospheric bottom reflectance data presented in this study.

This paper designs and develops an artificial neural network-based neural network corrector to perform secondary correction on the results of empirical inversion using remote sensing and geographic information systems due to the potential of neural networks to compensate for the inherent error of conventional empirical algorithms (GIS). As stated previously, the formula for calculating ANN is as follows:

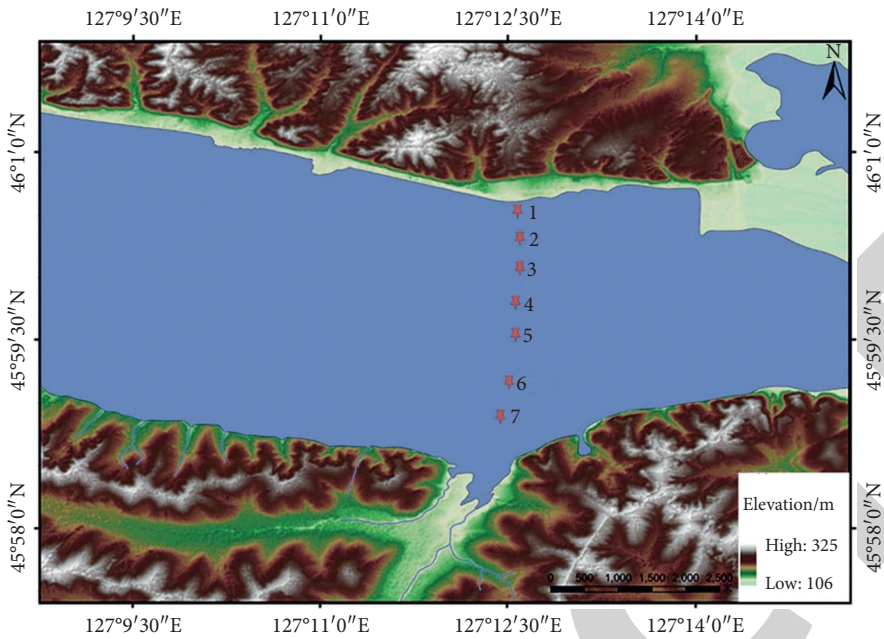

Figure 1: Sampling location for this article.

Table 1: SSC measured at 7 sampling points in dry season.

Point	Longitude and latitude	SSC
1	127°12′30″E/46°0′30″N	0.163
2	127°12′30″E/46°0′15″N	0.153
3	127°12′30″E/46°0′0″N	0.132
4	127°12′30″E/46°59′45″N	0.142
5	127°12′30″E/46°59′30″N	0.133
6	127°12′30″E/46°59′12″N	0.141
7	127°12′30″E/46°59′0″N	0.161

Table 2: SSC measured at 7 sampling points in wet season.

Point	Longitude and latitude	SSC
1	127°12′30″E/46°0′30″N	0.186
2	127°12′30″E/46°0′15″N	0.166
3	127°12′30″E/46°0′0″N	0.160
4	127°12′30″E/46°59′45″N	0.133
5	127°12′30″E/46°59′30″N	0.146
6	127°12′30″E/46°59′12″N	0.162
7	127°12′30″E/46°59′0″N	0.172

$$g(z) = \frac{1}{1 - e^{-z}}, \tag{1}$$

where $g(z)$ denotes the sigmoid function.

$$a^{(l+1)} = g\left(a^{(l)} b^{(l)} + b_0^{(l)}\right), \tag{2}$$

where $a^{(l)}$ represents the activate node, $b^{(l)}$ is the parameter matrix, $b_0^{(l)}$ is the bias value, l stands for moment l.

Then, we have

$$h_b(x) = a^{(3)}. \tag{3}$$

The loss is

$$\text{loss} = \frac{1}{N} \sum \left[-y^{(i)} \log\left(h_b\left(x^{(i)}\right)\right) - \left(1 - y^{(i)}\right) \log\left(1 - h_b\left(x^{(i)}\right)\right)\right], \tag{4}$$

where N is the number of samples, y represents the true value.

The regularized function [8] is

regularized loss,

$$= \frac{1}{N} \sum \left[-y^{(i)} \log\left(h_b\left(x^{(i)}\right)\right) - \left(1 - y^{(i)}\right) \log\left(1 - h_b\left(x^{(i)}\right)\right)\right] + c\left(y - y^{(i)}\right)^2, \tag{5}$$

where c is regularization parameter, N is the number of samples.

SSC is calculated as follows:

$$\text{SSC} = A * R(\text{Bestband}) + B, \tag{6}$$

where A and B are R^2.

4. Results

Ten of the thirteen bands on Sentinel-2A are used for atmospheric correction. It does not conduct correlation studies because the 10th band is used to correct the atmosphere. Beginning with the first band, the wavelength at the center of each succeeding band grows longer. In this case, the research band must be chosen from Band2, Band3, Band4, Band8, etc., [7, 10].

There are currently a variety of band combination techniques that can be used for SSC inversion, including single band, band ratio, and multiple band combination techniques. By adjusting the band ratio and employing a combination of multiple bands, it is possible to reduce the impact of water chlorophyll and other suspended contaminants on inversion results. In this article, single-band, band ratio, three-band combination, and four-band combination

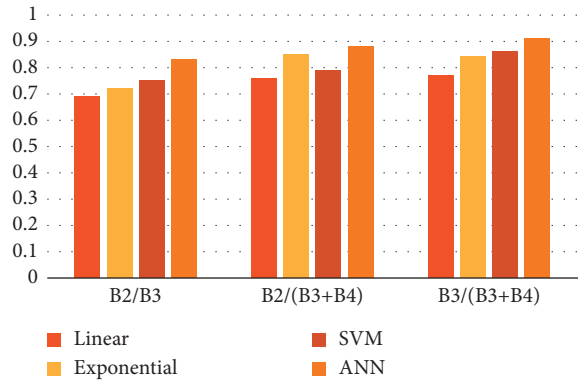

Figure 2: Model comparison of four models of R^2 during the dry season.

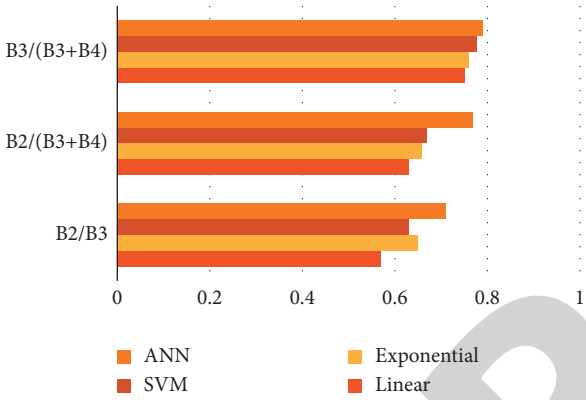

Figure 3: Model comparison of four models of R^2 during the wet season.

data are generated using the Band math tool in ENVI in conjunction with the SSC for correlation analysis. In general, regardless of whether it is a single Band8 near-infrared band or a band ratio and multiband combination involving the Band8 near-infrared band, the correlation between SSC and other wavelengths is relatively low. Possible explanations include the lower sediment concentration in the Songhua River, which indicates that the Band8 near-infrared band is insensitive to it, or the presence of organic matter such as chlorophyll in the sampling area, which interferes with the monitoring effect of the Band8 near-infrared band on SSC sand.

The evaluation indexes selected in this paper are RMSE, MAPE and R, and the calculation formula is as follows:

$$\text{MAPE} = \frac{1}{N}\sum\left|\frac{\hat{y}_i - y_i}{y_i}\right|,$$

$$\text{RMSE} = \left(\frac{1}{N}\sum(\hat{y}_i - y_i)^2\right)^{1/2}, \quad (7)$$

$$R^2 = \frac{\text{SSR}}{\text{SSE}},$$

where $\hat{y}_i$ is the predicted value of SSC.

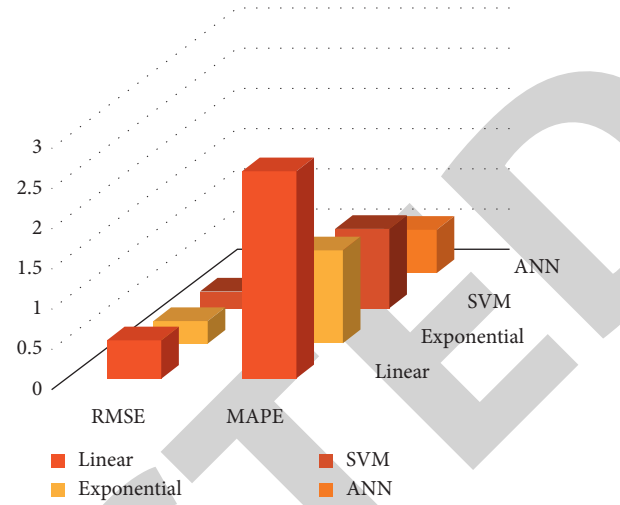

Figure 4: Model comparison of four models of RMSE and MAPE during the dry season.

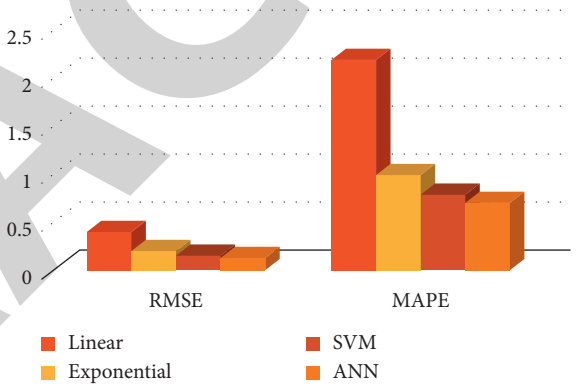

Figure 5: Model comparison of four models of RMSE and MAPE during the wet season.

According to the band correlation analysis, this paper selects the band combination with a correlation coefficient greater than 0.6 to establish the inversion model. The inversion model adopts ANN, linear model, exponential model, and SVM. Remote sensing reflectance as an independent variable and SSC as dependent variable. The results of correlation coefficient are shown in Figure 2 and Figure 3.

Figures 2 and 3 demonstrate that the fitting degree of the ANN model of B3/(B3 + B4) during drought conditions is the highest, and is 0.91. The SVM model is second, with a fitting degree of 0.86, and the linear model is the worst, with a fitting degree of 0.75. The fitting degree of the ANN model of B3 (B3 + B4) during the wet season is the highest, coming in at 0.791. The performance gap between the SVM and exponential model is negligible, with both models yielding roughly 0.765. Overall, the fitting degree of B2/B3 is lowest in the dry period and wet period, and the 0.57 fitting degree of the linear model is lowest in the wet period.

Figures 4 and 5 depict the results of comparisons of RMSE and MAPE for various time periods.

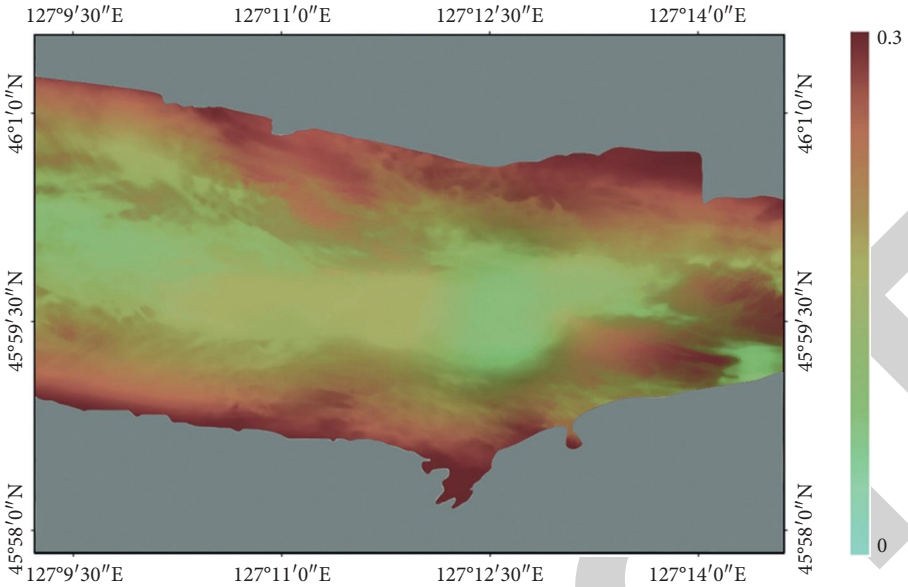

Figure 6: Inversion effect during the dry season.

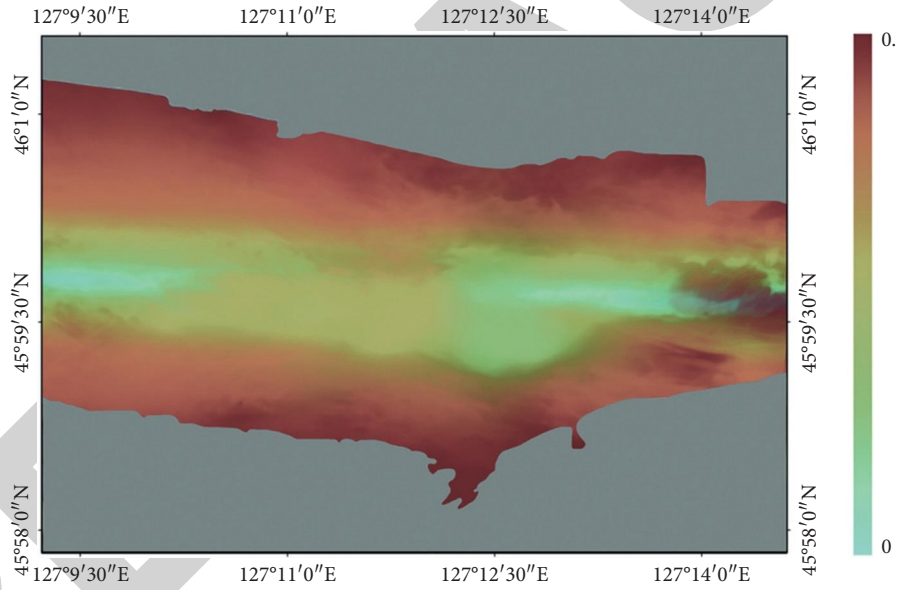

Figure 7: Inversion effect during the wet season.

As can be observed from Figures 4 and 5, the model suggested in this work is the lowest in both indicators, indicating that the performance of the model is the best. Specifically, in the drought era, the RMSE of ANN is 0.14, which is much lower than that of the linear model (0.48) and exponential model (0.19). (0.19). The MAPE of ANN is 0.54, whereas that of the linear model is 2.58 and SVM is 0.99 The results of the wet period are comparable. ANN has the best effect, followed by SVM, and the lowest is the linear model. The RMSE of the linear model is 0.40 and MAPE is 2.19, which are substantially higher than the other three models.

ENVI software produces the inversion results of SSC in different periods, as shown in Figures 5 and 6. After obtaining the inversion model for the dry season and wet season and verifying the accuracy of the model, the inversion results of SSC in different periods are produced are as shown in Figures 6 and 7.

5. Conclusion

This paper first introduces remote sensing and geographic information system (GIS) technology and then uses the sentinel-2 satellite with a resolution of 10 m after resampling to conduct an inversion and comparison study of SSC content in the upper reaches of a Chinese water control project during the wet and dry seasons. A neural network corrector based on artificial neural networks is also designed and developed to correct empirical inversion findings, which

is based on the ability of neural networks to compensate for the inherent error of the traditional empirical method. In this study, B2, B3, B4, and B8 are selected as inversion models to generate sensitive bands; these bands are then ratio-processed to generate inversion models, as described in the preceding section. The results indicate that the model has a high degree of accuracy, which can be used to reduce the model's inherent error and guarantee the accuracy of the inversion. It is found that the SSC is frequently larger during the wet season than during the dry season. The primary reason for this is that during the wet season, the rise in water level sends a substantial amount of sediment into the river, thereby increasing the sediment concentration in the river. Typically, the distribution of SSC in a river is characterized by a low concentration in the river's center and a high concentration on the riverbank. This is the most likely explanation, as silt is easily deposited on the bank due to the low velocity, and there are numerous other contaminants that affect remote sensing reflectance. As demonstrated by the inversion effect map, the SSC on the bank is quite high.

This article only analyzes the sediment deposition in a specific area, and the sediment deposition in the seaside is quite different from that in the river. In the future, we will further analyze the sediment deposition in the coastal area.

Data Availability

The data used to support the findings of this study are available from the corresponding author upon request.

Conflicts of Interest

The authors declare that there are no conflicts of interest.

Acknowledgments

The paper was supported by the Natural Science Research Project in Colleges and Universities of Anhui Province under Contract no. KJ2020A0719; the National Natural Science Foundation of China under Contract no. 41976187; the Science and Technology Planning Project of Chuzhou under Contract no. 2021ZD010; The Scientific Research Foundation of Chuzhou University under Contract no. 2020qd02.

References

[1] W. Halecki, E. Kruk, and M. Ryczek, "Estimations of nitrate nitrogen, total phosphorus flux and suspended sediment concentration (SSC) as indicators of surface-erosion processes using an ANN (Artificial Neural Network) based on geomorphological parameters in mountainous catchments," *Ecological Indicators*, vol. 91, pp. 461–469, 2018.

[2] A. M. Melesse, S. Ahmad, M. E. McClain, X. Wang, and Y Lim, "Suspended sediment load prediction of river systems: an artificial neural network approach," *Agricultural Water Management*, vol. 98, no. 5, pp. 855–866, 2011.

[3] M. B. Kazemzadeh, S. A. Ayyoubzadeh, and A. Moridnezhad, "Remote sensing of temporal and spatial variations of suspended sediment concentration in Bahmanshir Estuary, Iran [J]," *Indian Journal of Science and Technology*, vol. 6, no. 8, pp. 5036–5045, 2013.

[4] K. T. Peterson, V. Sagan, P. Sidike, A. Cox, and M Martinez, "Suspended sediment concentration estimation from landsat imagery along the lower Missouri and middle Mississippi rivers using an extreme learning machine," *Remote Sensing*, vol. 10, no. 10, p. 1503, 2018.

[5] M. E. Newcomer, A. J. M. Kuss, T. Ketron, A. Remar, V. Choksi, and J. W Skiles, "Estuarine sediment deposition during wetland restoration: a GIS and remote sensing modeling approach," *Geocarto International*, vol. 29, no. 4, pp. 451–467, 2014.

[6] Y. Chebud, G. M. Naja, R. G. Rivero, and A. M Melesse, "Water quality monitoring using remote sensing and an artificial neural network," *Water, Air, & Soil Pollution*, vol. 223, no. 8, pp. 4875–4887, 2012.

[7] H. O. Fagundes, F. M. Fan, and R. C. D. Paiva, "Automatic calibration of a large-scale sediment model using suspended sediment concentration," *Water Quality, and Remote Sensing Data*, RBRH, vol. 24, , 2019.

[8] B. D. Nguyen, N. A. Bui, and T. M. Dang, "Estimation of suspended sediment concentration in downstream of the Ba river basin using remote sensing images," *Inżynieria Mineralna*, vol. 3, 2021.

[9] S. Kanga, G. Meraj, B. Das, M. Farooq, S. Chaudhuri, and S. K Singh, "Modeling the spatial pattern of sediment flow in lower Hugli estuary, West Bengal, India by quantifying suspended sediment concentration (SSC) and depth conditions using geoinformatics," *Applied Computing and Geosciences*, vol. 8, Article ID 100043, 2020.

[10] J. L. Kong, X. M. Sun, D. W. Wong et al., "A semi-analytical model for remote sensing retrieval of suspended sediment concentration in the gulf of bohai, China," *Remote Sensing*, vol. 7, no. 5, pp. 5373–5397, 2015.

[11] A. R. Senthil Kumar, C. S. P. Ojha, M. K. Goyal, R. D. Singh, and P. K Swamee, "Modeling of suspended sediment concentration at kasol in India using ANN, fuzzy logic, and decision tree algorithms," *Journal of Hydrologic Engineering*, vol. 17, no. 3, pp. 394–404, 2012.

[12] Y. Zhang, J. Pulliainen, S. Koponen, and M Hallikainen, "Application of an empirical neural network to surface water quality estimation in the Gulf of Finland using combined optical data and microwave data," *Remote Sensing of Environment*, vol. 81, no. 2-3, pp. 327–336, 2002.

[13] Y. Zhang, J. T. Pulliainen, and S. S. Koponen, "Water quality retrievals from combined Landsat TM data and ERS-2 SAR data in the Gulf of Finland[J]," *IEEE Transactions on Geoscience and Remote Sensing*, vol. 41, no. 3, pp. 622–629, 2003.

[14] M. Rahman, G. M. Islam, and M. Rahman, *Remote Sensing for Monitoring Suspended Sediment Concentration in the Lower Ganges (Padma) River*, Springer, Berlin, Germany, pp. 183–196, 2021.

[15] Z. R. Womber, F. A. Zimale, M. G. Kebedew et al., "Estimation of suspended sediment concentration from remote sensing and in situ measurement over lake tana, Ethiopia," *Advances in Civil Engineering*, vol. 2021, pp. 1–17, Article ID 9948780, 2021.

[16] Y. Liu, M. A. Islam, and J. Gao, "Quantification of shallow water quality parameters by means of remote sensing," *Progress in Physical Geography: Earth and Environment*, vol. 27, no. 1, pp. 24–43, 2003.

[17] D. Kumar, A. Pandey, N. Sharma, and W. A Flugel, "Modeling suspended sediment using artificial neural networks and

TRMM-3B42 version 7 rainfall dataset," *Journal of Hydrologic Engineering*, vol. 20, no. 6, Article ID C4014007, 2015.

[18] V. V. Klemas, R. T. Field, and O. Weatherbee, "Remote sensing of coastal wetlands and estuaries," in *Proceedings of the 2004 USA-Baltic Internation Symposium*, pp. 1–3, IEEE, Klaipeda, Lithuania, June 2004.

[19] A. Mojtahedi, M. Dadashzadeh, M. Azizkhani, A. Mohammadian, and R Almasi, "Assessing climate and human activity effects on lake characteristics using spatio-temporal satellite data and an emotional neural network," *Environmental Earth Sciences*, vol. 81, no. 3, p. 61, 2022.

[20] R. R. Marinho, T. Harmel, J. M. Martinez, and N. P Filizola Junior, "Spatiotemporal dynamics of suspended sediments in the negro river, amazon basin, from in situ and sentinel-2 remote sensing data," *ISPRS International Journal of Geo-Information*, vol. 10, no. 2, p. 86, 2021.

[21] M. Newcomer, A. Kuss, T. Ketron, and J. W. Skiles, "Modeling sediment deposition for predicting marsh habitat development," in *Proceedings for the American Society for Photogrammetry and Remote Sensing Conference*, Milwaukee, Wisconsin, May 2011.

[22] G. Ebenezer Adjovu, S. Ahmad, and H. Stephen, "Analysis of suspended material in lake mead using remote sensing indices [C]//World environmental and water," *Resources Congress*, vol. 2021, pp. 754–768, 2021.

[23] C. Beveridge, F. Hossain, and M. Bonnema, "Estimating impacts of dam development and landscape changes on suspended sediment concentrations in the mekong river basin's 3S tributaries," *Journal of Hydrologic Engineering*, vol. 25, no. 7, Article ID 05020014, 2020.

[24] N. T. B. Phuong, N. B. Duy, and N. C. Nghiem, "Remote sensing for monitoring surface water quality in the Vietnamese Mekong delta: the application for estimating chemical oxygen demand in river reaches in Binh Dai, Ben Tre[J]," *Vietnam Journal of Earth Sciences*, vol. 39, no. 3, pp. 256–268, 2017.

[25] S. Kaliraj, N. Chandrasekar, and N. S. Magesh, "Multispectral image analysis of suspended sediment concentration along the Southern coast of Kanyakumari, Tamil Nadu, India[J]," *J. Coast. Sci*, vol. 1, no. 1, 2014.

[26] A. Amamra, K. Khanchoul, S. Eslamian, and S. H Zobir, "Suspended sediment estimation using regression and artificial neural network models: kebir watershed, northeast of Algeria, North Africa," *International Journal of Horticultural Science and Technology*, vol. 8, no. 4, p. 352, 2018.

[27] N. M. Dang, "Integration of ANFIS with PCA and DWT for daily suspended sediment concentration prediction," *[J]. Water SA*, vol. 47, no. 2, pp. 200–209, 2021.

[28] S. Shanmuga Priyaa and B. K. Jena, "Suspended sediments concentration on shoreline change using satellite images for southern Kerala coast," *Journal of Earth System Science*, vol. 130, no. 4, p. 211, 2021.

[29] P. R. Kadavi and C. W. Lee, "Land cover classification analysis of volcanic island in Aleutian Arc using an artificial neural network (ANN) and a support vector machine (SVM) from Landsat imagery," *Geosciences Journal*, vol. 22, no. 4, pp. 653–665, 2018.

[30] K. P. Sudheer, I. Chaubey, and V. Garg, "Lake water quality assessment from landsat thematic mapper data using neural network: an approach to optimal band combination SELECTION1," *Journal of the American Water Resources Association*, vol. 42, no. 6, pp. 1683–1695, 2006.

[31] M. Haghparast and M. Mokhtarzade, "Estimation of turbidity and chlorophyll a concentration in the Caspian Sea through time series analysis of satellite images and wavelet neural networks[J]," *Iranian Journal of Remote Sensing & GIS*, vol. 10, no. 1, pp. 91–108, 2018.

[32] J. F. Mas and J. J. Flores, "The application of artificial neural networks to the analysis of remotely sensed data," *International Journal of Remote Sensing*, vol. 29, no. 3, pp. 617–663, 2008.

[33] S. Elsayed, H. Ibrahim, H. Hussein et al., "Assessment of water quality in lake qaroun using ground-based remote sensing data and artificial neural networks," *Water*, vol. 13, no. 21, p. 3094, 2021.

[34] S. Mohamadpur, H. Rouhani, and H. Ghorbani Vaghei, "Sediment concentration modeling in rill flow using the Adaptive Nero Fuzzy Inference System (ANFIS) in semi arid region," *Journal of Range and Watershed Managment*, vol. 70, no. 1, pp. 219–234, 2017.

[35] K. Song, Z. Wang, and J. Blackwell, "Water quality monitoring using Landsat Themate Mapper data with empirical algorithms in Chagan Lake, China," *Journal of Applied Remote Sensing*, vol. 5, no. 1, Article ID 053506, 2011.

[36] X. Han and C. Du, "Retrieval of suspended sediment in Songhua River based on sentinel-2 satellite," *Journal of Physics: Conference Series*, vol. 2002, no. 1, (6pp), Article ID 012077, 2021.